Analysis of interface conversion processes of ballistic and diffusive motion in driven superlattices

Thomas Wulf,* Christoph Petri, Benno Liebchen, and Peter Schmelcher†
Zentrum für Optische Quantentechnologien, Universität Hamburg, Luruper Chaussee 149, 22761 Hamburg, Germany
(Received 7 March 2012; revised manuscript received 13 June 2012; published 2 July 2012)

We explore the nonequilibrium dynamics of noninteracting classical particles in a one-dimensional driven superlattice which is composed of domains exposed to different time-dependent forces. It is shown how the combination of directed transport and conversion processes from diffusive to ballistic motion causes strong correlations between velocity and phase for particles passing through a superlattice. A detailed understanding of the underlying mechanism allows us to tune the resulting velocity distributions at distinguished points in the superlattice by means of local variations of the applied driving force. As an intriguing application we present a scheme how initially diffusive particles can be transformed into a monoenergetic pulsed particle beam whose parameters such as its energy can be varied.

DOI: 10.1103/PhysRevE.86.016201 PACS number(s): 05.45.Ac, 05.45.Pq, 05.60.Cd

I. INTRODUCTION

Dynamical systems and their transport properties have been studied extensively over the last decades [1], whereas the topic stimulated a vast amount of research when the possibility of directed currents in the absence of a mean force was realized [2–4]. Since the second law of thermodynamics forbids such transport phenomena in equilibrium, these systems have to be constantly driven out of equilibrium. Early works [2–4] were based on noise, that is, statistical external fields, in combination with spatially asymmetric so-called "ratchet" potentials to overcome the limitations formulated by the second law of thermodynamics and thus to evoke a particle current. These types of systems are of particular interest because they outline a working principle for biological systems such as molecular motors [5,6] or quantum motors [7].

However, it was soon realized that directed currents can very well be obtained with deterministic external fields, as long as certain spatial and temporal symmetries in the equations of motion are broken [8], which was investigated afterward in a vast amount of literature (see [9–15] and references therein). These deterministic ratchets are of particular interest since they might have remarkable applications in nanoscale devices such as electron pumps or transistors [16]. First experimental realizations included semiconductors or semiconductor microstructures where a combination of laser fields has been applied which led to directed currents in electron ratchets [17,18]. Directed currents also became a subject of interest in experiments concerning cold atoms in optical lattices [19–22], where additional ac forces are applied to drive the system out of equilibrium and at the same time break the required symmetries that would otherwise prevent transport phenomena. These type of experiments are of particular interest since they allow for a precise control over the system parameters and provide extensive tunability in the used ac drivings [20,22].

While the so far mentioned works focus on only time-dependent ac forces, it was found recently that a spatial dependence of these ac forces leads to a diversity of dynamical phenomena [23–25]. The latter studies address the classical dynamics of particles in a lattice with a site-dependent driving. In [23] it is demonstrated how a phase-modulated lattice allows for directed transport even though the driving of each barrier on its own does not break the relevant symmetries [8]. Reference [24] shows how a ramping of the potential height in combination with a site-dependent driving leads to a patterned deposition of particles. A specific realization of a lattice with a site-dependent driving is the one of a block lattice (BL) as introduced in [25], which is reminiscent of semiconductor heterostructures and superlattices. Indeed, only recently the possibility of ratchet effects in superlattices of semiconductor heterostructures with a superimposed periodic potential was reported [26,27]. In the case of [25], the superlattice consists of different blocks containing many inidvidual barriers where the barriers of each block are governed by a certain time dependence, that is, driving law, whereas different blocks exhibit, in general, different driving laws. The long time transient dynamics in such a superlattice shows intriguing phenomena like the formation of spatial density oscillations. The latter were explained and analyzed by means of conversion processes from diffusive to ballistic (and vice versa) motion at the positions where two neighboring blocks connect, that is, at the interfaces of two blocks. However, a detailed analysis of the processes occurring in a unit cell of such a superlattice—that is a system containing only two blocks each equipped with one of the used driving laws—is still missing and is therefore subject of the present work. In this sense we investigate the diffusive to ballistic motion conversion processes in detail and explore their influence on the dynamics of particles leaving the two block system. As a result, we obtain peaked velocity distributions for outgoing particles even though their initial conditions are chosen exclusively within the chaotic sea of the underlying phase space. By adjusting parameters in the driving we are able to manipulate these velocity distributions in a controlled manner. Finally, we demonstrate how the insights gained from the two block system enable us to exploit the conversion processes in superlattices built up of many blocks, each equipped with a unique driving law. In doing so an initially diffusive particle ensemble is converted into an ensemble with a velocity distribution containing a single peak, whereas both the width as well as the peaks mean velocity can be tuned.

*Thomas.Wulf@physnet.uni-hamburg.de
†Peter.Schmelcher@physnet.uni-hamburg.de

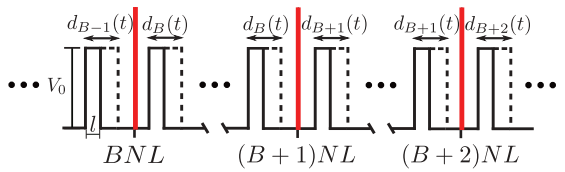

FIG. 1. (Color online) Sketch of a lattice that consists of differently laterally driven blocks, where the barriers with $NB \leqslant i < (B+1)N$ are equipped with the same driving law $d_B(t)$.

The present work is structured in the following way. In Sec. II we introduce the setup of a BL. In Sec. III the dynamics of a single block is discussed. We explore the conversion of diffusive to ballistic motion at distinguished positions in the BL in Sec. IV. Additionally, the influence of these processes for outgoing particles in a simple two block system is discussed in Sec. V. Finally, we investigate the dynamics of superlattices containing several hundred blocks in Sec. VI. Section VII contains our brief conclusions.

II. SETUP AND HAMILTONIAN

The system investigated is a one-dimensional driven lattice consisting of laterally oscillating square potential barriers of equal height V_0 and length l, as sketched in Fig. 1. Each barrier is characterized uniquely by its index i.

Furthermore, the barrier positions are time dependent and described by the so-called "driving law" $d(t)$, which is chosen such that the ith barrier remains at all times within an interval of length L expanding from iL to $(i+1)L$. Additionally, the lattice is divided into blocks such that different driving laws $d_B(t)$ (introducing the "block index" B) are used. In doing so, each $d_B(t)$ governs the barrier motions for the sites $NB \leqslant i < (B+1)N$ where N denotes the number of barriers within one block and is set to 10^4 throughout this work. The general structure of the driving law is a biharmonic function $d_B(t) = A_B[\cos(\omega_B t) + \sin(2\omega_B t + \Delta\Phi_B)]$ with three parameters A_B, ω_B, and $\Delta\Phi_B$ which depend on the block index B. Hence, the resulting classical Hamiltonian for noninteracting particles is given by

$$H(x,p,t) = \frac{p^2}{2m} + \sum_{B=0}^{B=N_{\mathrm{Bl}}-1} \sum_{i=BN}^{(B+1)N} \times V_0 \Theta(l/2 - |x - X_{0,i} - d_B(t)|), \qquad (1)$$

with N_{Bl} being the number of considered blocks and $X_{0,i}$ the equilibrium position of the ith barrier (chosen such that the barrier oscillates symmetrically within its unit cell, that is, $\min|X_{0,i} + d_B(t) - iL| = \min|X_{0,i} + d_B(t) - (i+1)L|$). Additionally, we set the mass $m = 1$ without loss of generality and keep $V_0 = 1.0$, $L = 5.0$, and $l = 1.0$ constant throughout this work.

III. DYNAMICS IN A SINGLE BLOCK

Even though the focus of this work is on composite systems consisting of multiple blocks exposed to different driving laws, these blocks are considered to be large in a sense that the dynamics of a particle within one block can be described by the Poincaré surfaces of section (PSS) as obtained by extending this block to an infinite uniformly driven lattice. It is therefore sensible to discuss the dynamical features such as the transport properties as well as the appearance of the PSS of the uniformly driven lattice. It is well established that the PSS for a uniformly driven lattice can be obtained by exploiting the temporal symmetry of the Hamiltonian: $H(x,t) = H(x,t+T)$. Thus, an appropriate choice for the PSS is given by $M = \{(x(t + kT) \bmod L,\ p(t+kT)) \mid k \in \mathbb{N}\}$, with $T = \frac{2\pi}{\omega}$ being the temporal period. According to this, we record the position taken modulo L and the velocity at certain times $2\pi k$, $k \in \mathbb{N}$ (and call this "position velocity section"). Such a PSS for $\omega = 1.0$, $A \approx 0.57$ and $\Delta\Phi = 0$ is shown in Fig. 2(b) and features the typical mixed phase space [28], that is, Kolmogorov–Arnold–Moser (KAM) islands embedded in a chaotic sea which is bounded by the first invariant spanning curve (FISC). Note that the white rectangle is caused by adding the potential energy for particles which are within a barrier at times when position and velocity are recorded. This is done to avoid discontinuities in the PSS caused by the discontinuous potential $V(x,t)$ (cf. [23]). For later usage we show additionally the position velocity section for parameters $\omega = 1.0$, $A \approx -0.57$, and $\Delta\Phi = 0$ in Fig. 2(a). Note that Figs. 2(a) and 2(b) show the PSS of the left block and right block, respectively, of the corresponding two block system (see Sec. IV).

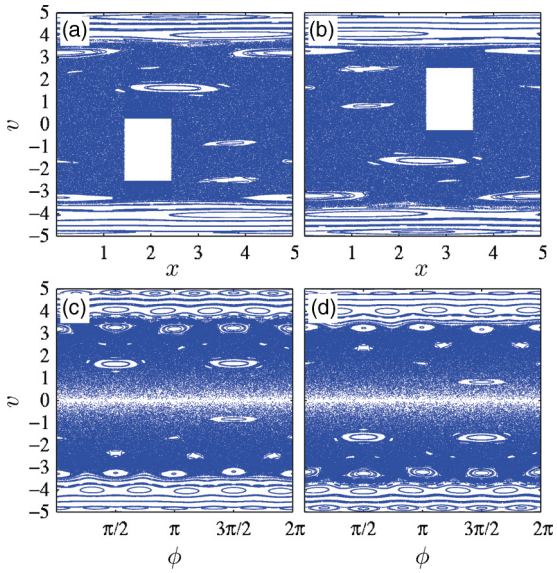

FIG. 2. (Color online) (a), (c) PSS for a uniformly driven lattice with parameters $A \approx -0.57, \Delta\Phi = 0$ and $\omega = 1.0$. (b), (d) PSS for $A \approx 0.57, \Delta\Phi = 0$ and $\omega = 1.0$. (a), (b) Position x taken modulo L as well as the velocity at times $\omega t \bmod 2\pi = 0$. (c), (d) Phases and velocities recorded at positions $x \bmod L = 0$.

A second possibility to illustrate the phase space of a uniformly driven lattice is given by the "phase velocity section" which exploits the spatial symmetry of the Hamiltonian: $H(x,t) = H(x+L,t)$. To this end we record the phases and velocities at certain positions iL. Hence, the PSS is obtained from the set of points $M = \{(t(x+kL) \bmod T,\ p(x + kL)) \mid k \in \mathbb{N}\}$ and the resulting plot is shown in Fig. 2(d) [again, the PSS for parameters as in Fig. 2(a) is shown

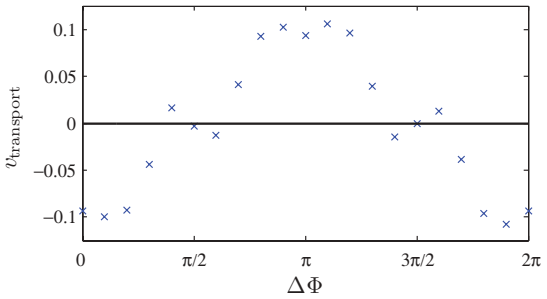

FIG. 3. (Color online) Numerically determined transport velocity as a function of $\Delta\Phi$ in an infinite uniformly driven lattice with $A \approx 0.57$ and $\omega = 1.0$.

additionally in Fig. 2(c) for later usage]. Apparently, it features qualitatively the same domains as the position velocity section [Fig 2(b)], that is, ballistic islands which are embedded in a bounded chaotic sea. However, in contrast to the previous case the chaotic sea appears to be nonuniformly filled with trajectories. This seeming contradiction to ergodicity can be resolved easily: According to ergodicity the chaotic sea in Fig. 2(b) can assumed to be filled with a uniform measure. Hence, the number of particles ΔN that pass $x_i = iL$ and therefore contribute to the phase velocity section per time Δt and velocity interval Δv is given by $\frac{\Delta N}{\Delta t} = \rho \frac{\Delta x}{\Delta t} \Delta v = \rho v \Delta v$, where Δx denotes the distance a particle travels in time Δt and ρ is the number of particles per phase space interval. Therefore, the number of particles passing x_i per velocity interval is $\frac{\Delta N}{\Delta v} = \rho v \Delta t$ and hence proportional to v. We now comment on the transport properties within a single block. For $\Delta\Phi_B \neq n\frac{\pi}{2}$ $(n \in \mathbb{Z})$ the biharmonic driving law breaks the time-reversal invariance as well as the parity symmetry of the Hamiltonian and the driven lattice allows for directed transport phenomena [8]. The transport as a function of $\Delta\Phi$ with fixed $A \approx 0.57$ and $\omega = 1.0$ is determined numerically by simulating 10^5 particles in a uniformly driven lattice for 10^6 barrier oscillations and calculating their average velocity after a certain transient time. The results are shown in Fig. 3 and appear to be in good agreement with the results of a symmetry analysis (cf. [8,29]) which yields $v_{\text{transport}} \propto -\cos(\Delta\Phi)$. However, there are noticeable deviations, for example, the reversed sign close to $\Delta\Phi_B = \pi/2$ and $\Delta\Phi_B = 3\pi/2$. Note that these deviations from a pure sinusoidal behavior should not surprise us, since a dependence of the transport on $\Delta\Phi$ as $v_{\text{transport}} \propto -\cos(\Delta\Phi)$ as derived in [8], is obtained from a first-order perturbative analysis of a system with a smooth potential instead of discontinuous potential barriers. As a matter of fact, the extension of the chaotic sea to positive or negative velocities, and hence the transport velocity, is a discontinuous function of any of the used parameters of the driving law and features "jumps" whenever a so far invariant torus is transformed into a penetrable chain of cantori under a small variation of one of the parameters of the driving law.

For a more detailed analysis of the dynamics in a uniformly driven lattice, we refer to [23] where this was done in great detail.

IV. INTERFACE CONVERSION IN THE TWO BLOCK SYSTEM

In Ref. [25] it was argued that a BL, as introduced in Sec. II, offers the opportunity for conversion processes from diffusive to ballistic motion and vice versa at interface positions where the driving law changes. These types of processes will be analyzed in detail throughout this section. We demonstrate in particular their influence on the velocity distribution of a particle ensemble.

A. Interface conversion

Let us introduce the simplest possible finite BL which is built up of only two blocks (i.e., $N_{\text{Bl}} = 2$) equipped with different driving laws. Such a system extends from $x_{\min} = 0$ to $x_{\max} = 2NL$ (so the simulation is stopped for a particle once it passes either of these positions) and the driving laws are $d_0(t)$ for $x < x_{\text{mid}} = NL$ and $d_1(t)$ for $x \geqslant x_{\text{mid}}$. The parameters of $d_1(t)$ are chosen as before ($\omega_1 = 1.0$, $A_1 \approx 0.57$ and $\Delta\Phi_1 = 0$) and thus the dynamics within the "right block" (RB) can be described by the two PSS in Figs. 2(b) and 2(d). Moreover, Fig. 3 reveals that the used driving law induces a negatively directed current. For the "left block" (LB) we chose $\omega_0 = 1.0$, $A_0 \approx -0.57$, and $\Delta\Phi_0 = 0$ yielding $d_0(t) = -d_1(t)$. Hence, the corresponding position-velocity section is given by Fig. 2(a) and the phase-velocity section is the one shown in Fig. 2(c). The induced current in the LB is therefore of the same magnitude as in the RB, but positively directed.

To understand how this setup allows for conversion processes it is helpful to consider the dynamics of a particle with initial conditions in the chaotic sea of the LB's phase space. Due to the positively directed current, this particle is, on average, transported toward x_{mid} and the chaotic sea for positive velocities in the corresponding phase velocity section [Fig. 2(c)] marks all possible phase space coordinates (v_D, ϕ_D) at which the particle can reach x_{mid} diffusively, while the coordinates belonging to ballistic motion (i.e., within ballistic islands or regular spanning curves above the FISC) (v_B, ϕ_B) are prohibited. However, once the particle passes the interface at x_{mid} its dynamics is no longer governed by the LB's phase space, but by the phase space of the RB, which is appropriately described by the PSS in Fig. 2(d). The crucial observation is that some of the coordinates (v_D, ϕ_D) belonging to diffusive motion in the LB correspond to ballistic motion in the RB. This is best seen by means of a concrete example: Imagine the particle reaches x_{mid} with $(v = 0.8, \phi = 3\pi/2)$, which is inside the chaotic sea of the LB's PSS [Fig. 2(c)]. For $x > x_{\text{mid}}$ the particles dynamics is described by the RB's PSS [Fig. 2(d)], where these coordinates correspond to a ballistic island. Hence, this initially diffusive particle would have become ballistic at the interface and we refer to this process as diffusive to ballistic motion conversion. Besides being injected into ballistic islands, the particles can equally well be injected into regular curves above the RBs FISC, because the FISC for positive velocities in the LB is at higher velocities as it is in the RB. To state a general rule, initially diffusive particles can be injected into every regular structure of the RB's PSS which has at least some "overlap" with the chaotic sea of

the LB's PSS. An example of a regular structure in which no injection can occur is the chain of ballistic islands at $v \approx 3.2$ in the RB's PSS [Fig. 2(d)]. These islands are "covered" by a chain of larger islands at the same velocity in the LB's PSS [Fig. 2(c)].

B. Density evolution in the two block setup

After having discussed the process of interface conversion in BLs, we will explore their influence on the time evolution of the particle density in the following.

To this end we propagate the dynamics of a particle ensemble in the two block system, which we introduced in Sec. IV A. As initial conditions we chose uniform distributions for the particles positions as well as their velocities with $0.4NL < x_{\mathrm{ini}} < 0.6NL$ and $-0.1 < v_{\mathrm{ini}} < 0.1$, respectively. Hence, the particles are symmetrically distributed around the LB's center and started in the chaotic sea of the phase space. Naively one might expect that due to the oppositely directed currents in the LB and the RB an accumulation of particles might happen at the interface at x_{mid}. As we see in the following, this does not occur due to the previously introduced conversion processes.

Figure 4 shows snapshots of the normalized particle density at different times. Figure 4(a) shows the particle density $\rho(x)$ for $t = 0$. For $t > 0$ the particle distribution starts to spread and reaches a Gaussian-like shape at $t = 10^4$ [Fig. 4(b)]. Afterward the ensemble drifts in positive x direction and once a sufficient amount of particles arrives at $x_{\mathrm{mid}} = 5 \times 10^4$ (marked by the red dashed line in Fig. 4) a sharp decrease of the density

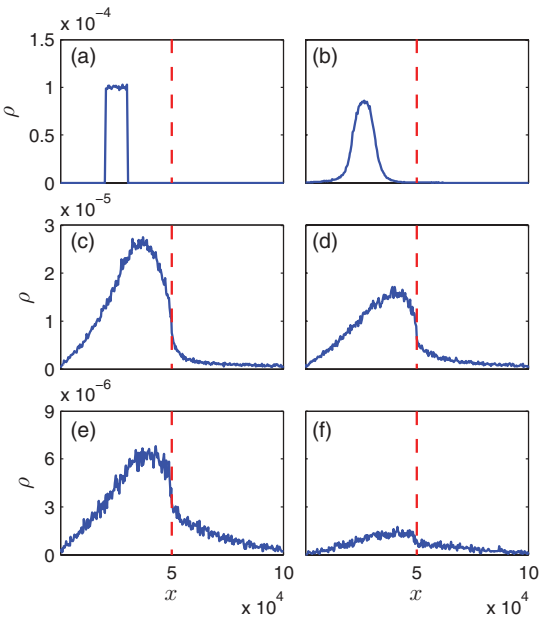

FIG. 4. (Color online) Particle density at different times in the two block setup ($N_{\mathrm{Bl}} = 2$) and $N = 10^4$, yielding $x_{\mathrm{mid}} = 5 \times 10^4$ (indicated by the red dashed line) and $x_{\mathrm{max}} = 10^5$. The two driving laws are $d_0(t)$ with $\omega_0 = 1.0$, $A_0 \approx -0.57$, and $\Delta\Phi_0 = 0$ for $x < x_{\mathrm{mid}}$ and $d_1(t) = -d_0(t)$ for $x > x_{\mathrm{mid}}$. All densities are normalized to the initial particle number 10^5. Snapshots of the particle density are shown for $t = 0$ (a), 10^4 (b), 10^5 (c), 1.8×10^5 (d), 3×10^5 (e), and 5.5×10^5 (f).

emerges at this position [Figs. 4(c) and 4(d)]. This effect outlasts until $t \approx 5.5 \times 10^5$ [Figs. 4(e) and 4(f)]. Finally at $t \approx 10^6$, all particles have left the system at either $x = x_{\mathrm{min}}$ or $x = x_{\mathrm{max}}$ and thus the density in the system is zero.

The broadening of the peak within the LB can be explained by underlying diffusion processes, because all particles are initially restricted to the chaotic sea. In fact, as long as the particles have not reached $x = x_{\mathrm{mid}}$ the ensemble is superdiffusive [23], leading to a fast expansion. On the one hand, the observed average drift of the ensemble in the LB is explained easily by the positively directed transport in the LB. On the other hand, the fast density decrease is—as mentioned before—somewhat counterintuitive. However, this effect is a straightforward consequence of the in Sec. IV A introduced conversion processes at x_{mid}. According to our discussion, the initially diffusive particles can be injected from the chaotic sea of the LB's PSS into regular structures of the RB's PSS which leads to a fast ballistic motion away from x_{mid}. If the particle remains diffusive, the directed transport brings it back to the interface and an injection from the chaotic sea of the RB to regular structures of the LB is possible. Hence, this process is repeated until an injection occurs and the particle leaves the system at x_{max} (or x_{min}) within a regular structure of the RB (or the LB). The fact that we do not observe a particle accumulation at the interface demonstrates that the conversion process from diffusive to ballistic motion happens on a sufficiently fast time scale to overcompensate accumulation effects caused by the directed currents.

C. Analysis of escaping particles in the two block setup

In the present section we investigate the conversion processes from diffusive to ballistic motions further and illustrate an intriguing hallmark of these processes, namely their influence on the particles phase-velocity distribution.

The starting point is the same two block setup as before and the initial conditions are chosen as before, too. However, instead of discussing the particle positions at certain times as we did in Sec. IV B, we now record the particle velocities and phases at distinguished positions: x_{min} and x_{max}. To this end the phase ϕ and the velocity v for every particle at x_{max} are recorded and the result is shown in Fig. 5(a). In the low velocity regime ($v \lesssim 3.0$) a distinguished island structure is apparent, whereas for higher velocities ($v \gtrsim 3.5$) the particles possess all possible phases from $\phi = 0$ to $\phi = 2\pi$. In between ($3.0 \lesssim v \lesssim 3.5$) the particles appear to have randomly distributed phases and velocities, but do not occupy certain islands.

The islands in the low velocity regime are evidently a consequence of the diffusive to ballistic motion conversion processes. Once a particle which comes from the LB is injected at $x = x_{\mathrm{mid}}$ into a regular structure of the RB, it cannot become diffusive again and travels to $x = x_{\mathrm{max}}$ ballistically. Moreover, it is unlikely for a diffusive particle to reach x_{max}, and indeed impossible if the length of the block tends to infinity, because the local current in the RB is negative. Hence, almost every particle in the velocity regime $v \lesssim 3.0$ in Fig. 5(a) is a ballistic one. Note that the island structures can easily be identified with the ballistic islands in the RB's PSS [Fig. 2(d)]. In an analogous way we can understand the velocity regime $v \gtrsim 3.5$: These particles are injected into surface spanning curves above

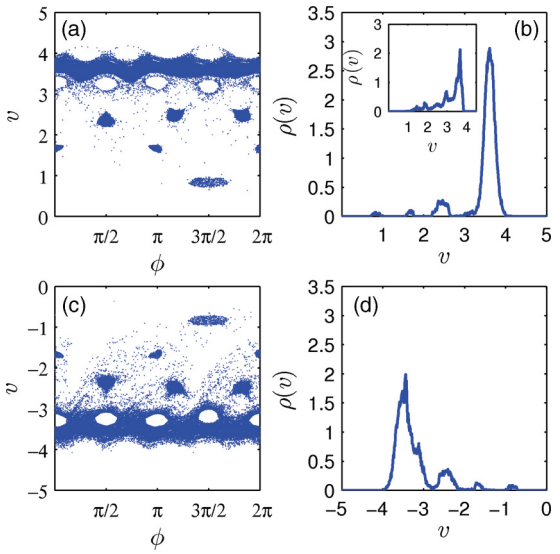

FIG. 5. (Color online) Properties of the escaping particles for the two block setup with the same parameters as in Fig. 4. (a) Phases and velocities at $x = x_{\max}$ and (c) at $x = x_{\min}$. (b),(d) The corresponding normalized velocity distributions $\rho(v)$. The inset in (b) shows the velocity distribution for particles which arrive at $x = x_{\mathrm{mid}}$ for their first time.

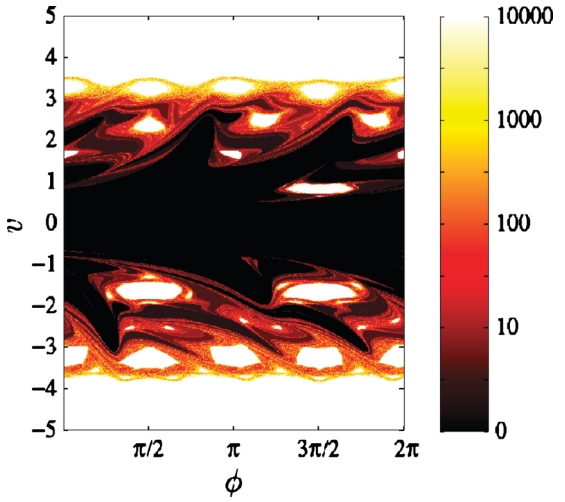

FIG. 6. (Color online) Length of Lévy flights for particles exhibiting chaotic dynamics in a uniformly driven lattice with driving law $d_1(t)$ [parameters as in Fig. 2(d)]. The white regions correspond to initial conditions leading to regular motion.

the RB's FISC at x_{mid}. Accordingly, they are not restricted to certain phases.

The explanation why certain islands in the velocity regime $3.0 \lesssim v \lesssim 3.5$ are avoided by particles at $x_{\max}$ can be given straightforwardly after our previous discussions on the conversion process. As already mentioned in Sec. IV A, these islands correspond to regular structures of the PSS in the RB which have no overlap with the chaotic sea of the LBs phase space and hence no injection occurs.

Finally, we turn our focus on the spread particles with $3.0 \lesssim v \lesssim 3.5$: A comparison with the corresponding PSS [Fig. 2(d)] reveals that these particles are located within the chaotic sea. Thus, they have indeed passed the RB contrariwise to the directed current. To understand why this occurs predominantly in this velocity regime, a short detour on the typical length of Lévy flights in the driven lattice is necessary. To this end we have simulated particles in a uniformly driven lattice with driving law $d_1(t)$ starting at $x = 0$ with 2×10^6 different initial conditions covering the phase space interval $(0 \leqslant \phi_{\mathrm{ini}} \leqslant 2\pi, \quad -5 \leqslant v_{\mathrm{ini}} \leqslant 5)$. For every initial condition the number of barriers that the particle passes, before the sign of its velocity changes, is recorded and shown in Fig. 6 (initial conditions leading to regular motion were excluded and are shown in white). Apparently, the number of passed barriers before the velocity is reversed can differ by several orders of magnitude and strongly depends on the initial condition. Most interesting for our purpose is the observation that particles started in the velocity regime $3.0 \lesssim v \lesssim 3.5$ exhibit extraordinarily long "ballisticlike" flights, which can be on the order of a few thousand barriers. Hence, it is more likely for a particle that remains diffusive once it passes x_{mid} to reach $x_{\max}$ before being transported back to x_{mid} if it is within this region of extraordinarily long Lévy flights. Indeed, a comparison of Fig. 6 with Fig. 5(a) reveals that the regions of long Lévy flights coincide with the ones where diffusive particles reach $x_{\max}$.

Even though the overall appearance of the plot shown in Fig. 6 does strongly depend on the used parameters in the driving law, it is—for later usage—worth emphasizing that the tendency for fast particles to exhibit much longer Lévy flights than slower ones is a rather general feature in the driven lattice. This is mainly caused by two facts: First, the lattice becomes a smaller perturbation for faster particles. Hence, the average velocity change at a collision with a barrier is small for a particle which is close to the FISC (note that it is indeed zero for particles on the FISC) and as a consequence it takes many collisions with the barrier before a notable impact on the particle velocity occurs. Second, for particles with large initial velocities it is likely to become sticky to the FISC which—according to the discussions in [23]—leads to long ballistic flights.

Besides leaving the system at $x_{\max}$, there is also the possibility for a particle to leave the system at $x_{\min}$. Again, phase and velocity at this particular position are recorded and shown in Fig. 5(c). This plot features qualitatively the same occupied domains as the one for $x_{\max}$ but now mirrored at $v = 0$: distinguished island structures belonging to a regular ballistic dynamics for less negative velocities, particles obeying chaotic dynamics which avoid ballistic islands for $-3.5 \lesssim v \lesssim -3.0$, and particles on regular spanning curves with velocities $v \lesssim -3.5$. The main difference appears to be the larger amount of spread diffusive particles for velocities with $v \gtrsim -3$ which do not correspond to ballistic islands.

Both the difference as well as the similarity to the $x_{\max}$ plot can be understood intuitively: Since the ensemble is initially located around the center of the LB, the number of barriers that these particles have to pass diffusively and opposite to the direction of the local current is roughly 5000, while it would be 10 000 for particles that have reached x_{mid}. Consequently, most of the spread diffusive particles seen in Fig. 5(c) are particles which have never reached x_{mid}. In contrast to this,

the particles reaching $x_{\min}$ within either ballistic islands or regular spanning curves have obviously passed x_{mid} at least twice, because otherwise they could not be injected into the corresponding regular structures of the LB. Note that once a particle reaches x_{mid}, it is injected into the PSS of the RB with $d_1(t)$ for positive velocities and into the PSS of the LB with $d_0(t)$ for negative velocities. Since we chose $d_0(t) = -d_1(t)$, the ballistic islands apparent in Fig. 5(c) are the same as in Fig. 5(a), but mirrored at $v = 0$.

D. Injection probabilities into different regular structures

So far we have seen that the two block system allows for diffusive to ballistic motion conversion processes. In this section we further investigate this phenomenon and discuss how likely injections into different regular regimes such as ballistic islands or spanning curves above the FISC are.

To get some insight it is instructive to compare the normalized phase integrated velocity distributions at $x_{\max}$ [Fig. 5(b)] with the one at $x_{\min}$ [Fig. 5(d)]. For our purpose crucial observation is that the peak at high velocities ($|v| \gtrsim 3$) is less pronounced at $x_{\min}$ and that the peaks corresponding to the ballistic islands appear slightly more populated (hardly visible) compared to the peaks in the distribution at $x_{\max}$. This effect can partially be explained by the larger number of diffusive particles at $x_{\min}$, leading to a broadening of the high velocity peak, but is also caused by certain characteristics of the injection process at x_{mid}, as we explain in the following.

A further understanding can be obtained by considering the velocity distributions for outgoing particles for a given number of times a particle has crossed x_{mid} before it leaves the system (in the following we refer to this number as n_{cr}) as shown in Fig. 7. Apparently, for $n_{\mathrm{cr}} = 1$ [Fig. 7(a)] the distribution features a very pronounced peak at velocities between 3 and 4, which appears stronger populated compared to the peak in the total velocity distribution at $x_{\max}$ shown in Fig. 5(b). On the contrary, the peaks corresponding to ballistic islands at smaller velocities are clearly more weakly pronounced. In the $n_{\mathrm{cr}} = 2$ case it is less apparent, but the islands at small velocities are still less pronounced as for the total distribution in Fig. 5(d). For $n_{\mathrm{cr}} = 3$ this effect is reversed and the low velocity peaks contain relatively more particles than they do in the total velocity distribution. Finally, particles leaving the system with $n_{\mathrm{cr}} = 4$ are very similar to the ones with $n_{\mathrm{cr}} = 3$ and no obvious deviation in the velocity distributions is observed. It will become clear later that this behavior is strongly correlated with a different effect which is worth mentioning at this point: Not only do the normalized distributions differ for different n_{cr}, but the probabilities for a particle to leave the system after a certain number of crossing n_{cr} are different as well. Hence, the injection probabilities into any kind of regular structure $p_{n_{\mathrm{cr}}}$ has to be different for different n_{cr} and we indeed found numerically that the probability for a particle to be injected into a regular structure while it passes x_{mid} for the first time is $p_1 \approx 0.49$, while it is $p_2 \approx 0.24$ for the second passing of x_{mid} and approximately $p_i \approx 0.15$ for $n_{\mathrm{cr}} > 2$.

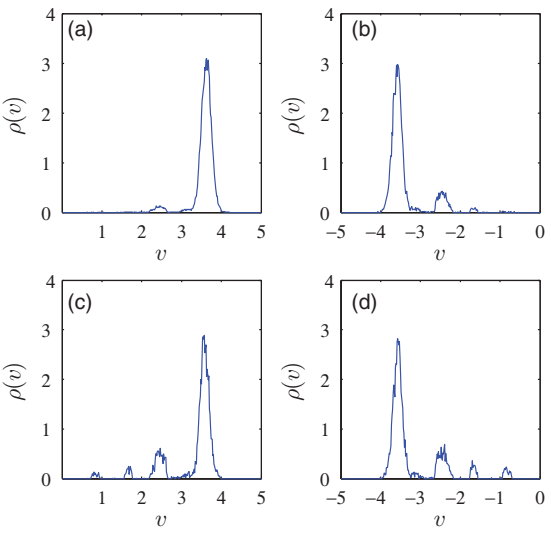

FIG. 7. (Color online) Normalized and phase integrated velocity distributions at $x_{\max}$ in (a) and (c) and at $x_{\min}$ in (b) and (d) for the subset of the ensemble which has crossed x_{mid} n_{cr} times (a) $n_{\mathrm{cr}} = 1$, (b) $n_{\mathrm{cr}} = 2$, (c) $n_{\mathrm{cr}} = 3$, and (d) $n_{\mathrm{cr}} = 4$. Parameters are as in Fig. 4.

To understand both the different overall injection probabilities $p_{n_{\mathrm{cr}}}$ for different n_{cr} as well as the different appearances of the corresponding velocity distributions, an argument which combines the length of Lévy flights in different regions of the phase space (as discussed before and shown in Fig. 6 for the RB and to be mirrored at $v = 0$ for the LB) together with the ergodicity property is required: Due to ergodicity parts of the phase space corresponding to long ballistic flights must be visited less frequently, but once a particle gets there, it stays for a comparably long time. Hence, a particle initially started very close to x_{mid} with a small velocity, reaches the interface after only a few collisions and, as a consequence, it is unlikely to reach the high velocity regime for such a particle. On the contrary, for a particle that started far—say some thousand barriers—away from x_{mid}, it is likely that the particle reaches this high velocity domain at some point. Once it possesses such a high velocity, the length of its Lévy flight is of the same order as its distance from x_{mid} and the particle typically reaches the interface while being still confined to this domain of phase space. We remark that this effect can easily be observed in the velocity distribution at x_{mid} for particles which reach this position for their first time as shown in the inset of Fig. 5(b). Apparently, the distribution reveals a strongly pronounced peak at velocities close the LBs FISC, in agreement with the previous discussion. Since these fast particles in the LB have velocities $v \gtrsim 3.5$ they are injected into regular spanning curves above the FISC of the RB, which explains why particles at the first injection process have extraordinarily high velocities and consequently why p_1 is extraordinarily large. Additionally, it illustrates why this domain appears to be strongly populated for $n_{\mathrm{cr}} = 1$ [cf. Fig. 7(a)].

Following the same arguments, the velocity distribution for $n_{\mathrm{cr}} = 2$ as well as the slightly enhanced value of p_2 compared to p_i with $i > 2$ can be understood too. Because the particles are extraordinarily fast at their first arrival at x_{mid}, a comparably large fraction of particles which remain diffusive is injected into the part of the RBs PSS corresponding to long Lévy flights (cf. Fig. 6). Hence, they surpass a large number of barriers in the RB, which is on the order of 10^3 before their velocity is reversed for the first time. Afterward, they are most likely

transported toward x_{mid} due to the negatively directed current in the RB. Now the same argument as before holds: Because these particles are relatively far away from x_{mid}, they reach x_{mid} predominantly with a high velocity. Hence, this domain is still strongly populated for the $n_{\mathrm{cr}} = 2$ injection process and p_2 is slightly enhanced. By now most of the fast particles have left the system and the still diffusive ones are transported back to x_{mid} after only a few collisions. Consequently, the injection probability into the high velocity domain is suppressed for larger n_{cr}.

V. CONTROLLING THE VELOCITY DISTRIBUTION

We have seen in Sec. IV that a BL consisting of differently driven blocks allows for the conversion of diffusive to ballistic motion and vice versa at interfaces where the driving law changes. As a hallmark of these processes, we obtained velocity distributions with pronounced peaks at the velocities associated with regular structures in the underlying phase space. In this section we provide an overview of the question as to what extent these conversion processes can be exploited to modulate the velocity distribution for outgoing particles by adjusting parameters in the driving law.

Again we focus on the two block setup ($N_{\mathrm{Bl}} = 2$, $N = 10^4$) with two different driving laws $d_0(t)$ for $x < x_{\mathrm{mid}}$ and $d_1(t)$ for $x \geqslant x_{\mathrm{mid}}$. The parameters in $d_0(t)$ remain as before and thus a positively directed current is induced in the LB. On the contrary, each parameter in $d_1(t)$ is varied separately and its influence on the velocity distributions at x_{max} and x_{min} is studied. To this end we propagate an ensemble of 10^5 particles (initial conditions as in Sec. IV) until all particles left the two block system. The phase integrated velocity distributions for particles which leave the system at x_{max} are shown as color plots for three different parameter regimes in Fig. 8.

For a varying frequency ω_1 (and fixed A_1 and $\Delta\Phi_1$), the results are shown in Fig. 8(a). Evidently, the particles arrive at x_{max} within a broad range of velocities for small frequencies in the RB, while they are restricted to certain comparably narrow velocity intervals at higher values of ω_1. A similar behavior can be observed for variations in the amplitude of the driving [Fig. 8(b)]. Analogous to the frequency dependence, the particles cover a broad velocity interval ($1.5 \lesssim v \lesssim 4.0$) for small amplitudes. With increasing A_1 this interval decreases and additional narrow velocity intervals emerge. However, these velocity intervals are rather unaffected by changes in A_1, which is in contrast to the frequency domain where their mean velocities tend to increase linearly with ω_1 [cf. Fig. 8(a)]. This difference can be understood by the fact that these velocity intervals correspond to ballistic islands in the RB's PSS (as explained in Sec. IV). Furthermore, these ballistic islands correspond to trajectories synchronized with the barrier oscillations in a way that every collision with the barrier occurs at distinguished phases. Each island is thereby characterized by its winding number n, which is defined (within a block) as the number of unit cells the particle passes within one period T. Hence, the average velocity of a particle trapped in such an island is given by $v_n = \frac{Ln}{T} = \frac{Ln}{2\pi}\omega_1$ and thus proportional to ω_1 and—at least within this simple picture—independent of A_1.

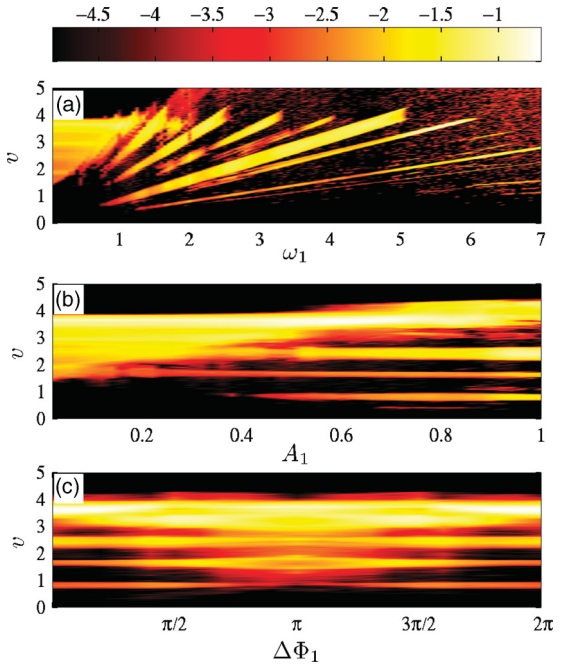

FIG. 8. (Color online) Phase-integrated velocity distributions at x_{max} (setup as as in Fig. 4) on a logarithmic scale for variations of (a) ω_1, (b) A_1, and (c) $\Delta\Phi_1$. Remaining parameters are as in Fig. 4.

Finally, Fig. 8(c) shows the velocity distribution as a function of $\Delta\Phi_1$ and reveals an increasing amount of diffusive particles for $\Delta\Phi_1$ close to $\Delta\Phi_1 = \pi$ compared to $\Delta\Phi_1 = 0$ (or $\Delta\Phi_1 = 2\pi$). This is a consequence of the dependence on $\Delta\Phi$ of the direction of the current in the RB (cf. Fig. 3), which is positively directed for $\Delta\Phi_1 = \pi$ while it is negatively directed for $\Delta\Phi_1 = 0$. Hence, more diffusive particles manage to traverse the RB for $\Delta\Phi_1 \approx \pi$.

At this point we would like to stress that from the discussion given in Sec. IV, the transmission through the RB with arbitrary parameters can be understood by means of its PSS in the following way: Assuming a negatively directed current in the RB, we can expect that the particles arrive at x_{max} predominantly within either ballistic islands or regular curves above the FISC corresponding to the RBs phase space. Hence, the phase velocity distributions at x_{max} provide an "image" of all the regular structures in the PSS of the RB which have overlap with the chaotic sea of the LB's PSS [Fig. 2(c)]. In addition to the ballistic particles some diffusive particles are expected to reach x_{max} if the underlying phase space of the RB possesses regions of long Lévy flights. In the case of a positively directed current in the RB, one has to take into account, that a large amount of particles traverses the RB diffusively.

VI. VELOCITY DISTRIBUTIONS IN SUPERLATTICES

In the previous sections we have demonstrated how a setup built up out of two blocks with different driving laws allows for conversion processes from diffusive to ballistic motion. Even more, we were able to control the velocity distributions for outgoing particles at x_{max} by adjusting parameters in the RB. In the following we argue how the so far gained insights can be exploited to maintain monoenergetic pulsed particle beams

out of diffusive particle ensembles in superlattices containing a few hundred blocks. The general outline of the used scheme is as follows. We start with an initially diffusive particle ensemble in the $B = 0$ block (with B being the block index; cf. Fig. 1) which is transported toward a first interface where particles can be injected into ballistic islands of the $B = 1$ blocks phase space. The parameters in the driving laws are chosen such that these now ballistic particles travel opposite to the directed currents and thus we obtain a peaked velocity distribution at the end of the $B = 1$ block. For the following blocks with $B = 2, \ldots, 100$ we show how the width of each peak in the velocity distribution can be tuned by adjusting the amplitude of the barrier oscillation blockewisely. As a last step, we demonstrate how an appropriate choice in the driving laws for $B > 100$ makes it possible to preserve one of the peaks in the velocity distributions while the other peaks are subsequently removed. Thus, we obtain a monoenergetic particle beam for outgoing particles in the superlattice. Moreover, the beam is pulsed in a sense that the particles leave the systems only at distinguished phases.

A. Interface dynamics of ballistic particles

Before we start a detailed discussion of the physics in the BL containing a few hundred blocks, let us again consider the simple case of a two block setup to introduce a new type of conversion processes which occurs in larger BL namely ballistic to ballistic or ballistic to diffusive conversion. To make our discussion more concrete we consider again a setup with driving laws as in Sec. IV. Hence, the PSS for the LB is shown in Fig. 2(c) and the PSS for the RB is shown in Fig. 2(d). In contrast to the previous discussions we explore the possible conversion processes for a ballistic particle arriving at the interface. For example, consider a particle beam started at $x_{\min}$ which uniformly occupies the ballistic island at $(v = 1.8, \phi = 3\pi/2)$ [in Fig. 2(c)] and passes ballistically the LB. Apparently, these particles would be entirely injected into the chaotic sea of the PSS in the RB once they pass x_{mid}. Due to the negatively directed transport in the RB the particles are transported back to x_{mid} where they can again be injected into any regular structures of the PSS corresponding to the LB, or after several passings of x_{mid} into regular structures of the RB. Hence, the outgoing particles at $x_{\max}$ for this initially monoenergetic beam would occupy all accessible regular structures of the PSS of the RB and the corresponding velocity distribution at $x_{\max}$ would contain multiple peaks.

As a second example we consider a particle beam (again started at $x_{\min}$) which passes the LB by uniformly occupying the ballistic island at $(v = 3.2, \phi = 3\pi/2)$. In this case, some particles are injected into the ballistic island in the RBs PSS at similar coordinates, while others become diffusive. The particles which remain ballistic traverse the RB and cause a dominant peak in the velocity distribution at $x_{\max}$. For the particles which become diffusive the same arguments hold as before. Thus, these particles lead to less pronounced peaks in the velocity distribution at velocities corresponding to any kind of regular structure in the RB. Accordingly, the initial particle beam was converted into a particle beam with a smaller width, because the ballistic island in the LB, that is, for the initial beam, is larger than the island in the RB in which these particles are injected. In addition to this, peaks in the velocity distribution emerge due to injection of diffusive particles after multiple crossings of x_{mid}.

B. Amplitude variations in superlattices

In the following section we demonstrate how the previously discussed interface dynamics of ballistic particles can be exploited to narrow the velocity distribution of particles in an appropriately designed superlattice. To this end we consider a setup built of $N_{\mathrm{Bl}} = 101$ blocks (whereas each block contains $N = 10^4$ barriers) which expands from $x_{\min} = 0$ to $x_{\max} = NLN_{\mathrm{Bl}}$. Accordingly, the positions of the interfaces, that is, the positions where the driving laws change, are given by $x_B = NLB$ with $B = 1, \ldots, 100$. For the $B = 0$ block the driving law is $d_0(t)$ with parameters as in Fig. 2(c) inducing a positively directed current. For $B = 1, \ldots, 100$ the driving laws are $d_B(t) = A_B[\cos(2.2t) + \sin(4.4t)]$ with $A_B = 0.3 + 0.07 \times B$ (i.e., the amplitude is slowly increased from 0.3 to 1.0), inducing negatively directed currents. The initial conditions for the simulated ensemble are $t = 0$, $0.4NL < x < 0.6NL$ and $-0.1 < v < 0.1$. Hence, the particles are located within the chaotic sea of the $B = 0$ block with driving law $d_0(t)$ and transported toward the first interface at $x_1 = NL$. At this point they can be injected into ballistic islands of the phase space in the $B = 1$ block. Since the local current in this block is negatively directed, it is hard to surpass for diffusive particles and we obtain a peaked velocity distribution at $x_2 = 2NL$ [Fig. 9(a)] which is is dominated by a peak at $v \approx 3.5$ and a less pronounced one at $v \approx 1.8$. The phase velocity distribution at $x_2 = 2NL$ [Fig. 10(a)] reveals that the dominant peak ($v \approx 3.5$) can be related to an island with winding number $n = 2$, while the second peak ($v \approx 1.8$) is associated with a $n = 1$ island.

In the following blocks the amplitude of the barrier oscillation is subsequently increased and as a result we obtain a velocity distribution with two narrow peaks at the same velocities as before for particles at $x_{\max} = 101NL$ [Fig. 9(b)]. Additionally, we observe some particles with velocities $v > 4.5$. The reason for the two dominant peaks is that the amplitude has (as

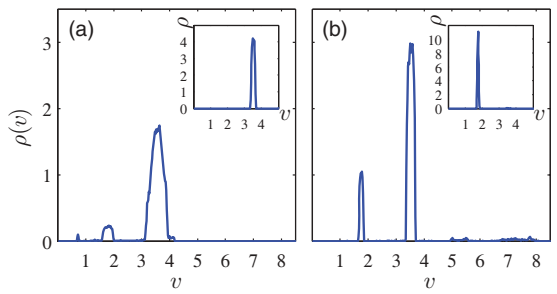

FIG. 9. (Color online) Velocity distributions at positions (a) $x_2 = 2NL$ and (b) $x_{\max} = 101NL$. Parameters in $d_0(t)$ are as in Fig. 4. For $0 < B \leqslant 100$ we set $d_B(t) = A_B[\cos(\omega_B t + \varphi_B) + \sin(2(\omega_B t + \varphi_B))]$ with $\omega_B = 2.2$, $\varphi_B = 0$, and $A_B = 0.3 + 0.07(B - 1)$. The inset in (a) shows $\rho(v)$ at $x = 200NL$ with $\omega_B = 2.2$, $A_B = A_{101}$, and $\varphi_B = \pi(B - 1)$ for $100 < B \leqslant 200$. The inset in (b) shows $\rho(v)$ at $x = 500NL$ with $\omega_B = 2.2$, $A_B = A_{101}$, and $\varphi_B = 0.02\pi(B - 1)$ for $100 < B \leqslant 500$.

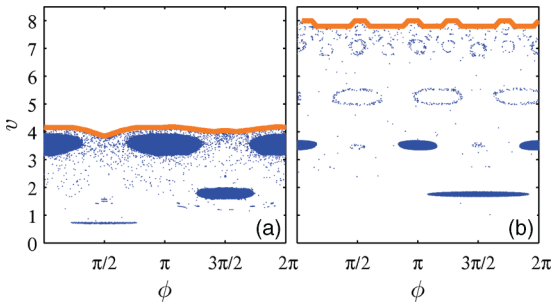

FIG. 10. (Color online) Phase velocity distributions at (a) $x = 2NL$ and (b) $x = 101NL$. Orange lines indicate the FISC (parameters as in Fig. 9).

argued in Sec. V) only little influence on the position of ballistic islands in phase space. Thus, most particles remain ballistic at each interface. However, the amplitude does have a notable influence on the size of the islands and by choosing the amplitude appropriately, one can tune the width of the velocity distribution by adjusting the size of the corresponding ballistic islands. In the present setup we exploit that an increasing amplitude leads to a decreasing size of the islands for the used parameters. Hence, the velocity distribution is squeezed when the particles propagate further into the superlattice. The fast particles with $v > 4.5$ correspond to particles in ballistic islands of the underlying phase space which is best seen in the phase velocity distribution at $x = 101NL$ [Fig. 10(b)]. In fact, these are the peaks in the velocity distribution discussed in the previous section that emerge due to injection of diffusive particles after multiple crossings of an interface.

C. Peaked velocity distributions in superlattices

The last step to a monoenergetic particle beam is to remove one of the peaks in Fig. 9(b) without losing too many particles in the other one. This can be done by exploiting the symmetries of both islands, which is achieved by adding more blocks to the superlattice with driving laws: $d_B(t) = 1.0[\cos(2.2t + \varphi_B) + \sin(4.4t + 2.2\varphi_B)]$ for $101 < B < 201$, with $\varphi_B = \pi(B - 1)$. Before we show the resulting velocity distributions, let us briefly discuss the idea behind the chosen driving laws: On the one hand, we have seen that the peak at $v \approx 3.5$ corresponds to a $n = 2$ island and consists of two island structures at the same velocity but at different phases (cf. Fig. 10). Hence, an additional phase shift $\varphi = \pi$ in the driving law "maps" both islands into each other and most particles remain ballistic. On the other hand, the $n = 1$ island which is responsible for the peak at $v \approx 1.8$ is "mapped" into the chaotic sea for such a phase shift and particles in it become diffusive. Even though some of these now diffusive particles might be reinjected into a ballistic island of the following block, the majority is transported away. Consequently, after performing this procedure multiple times, one obtains a monoenergetic particle beam. The resulting velocity distribution is shown in the inset of Fig. 9(a) and reveals that we obtain indeed the desired form of a monoenergetic particle beam.

At this point we remark that the described technique of removing peaks according to the symmetry of their associated ballistic island works for a wide range of different parameter values, as well as for ballistic islands with higher winding numbers. Unfortunately, it does not apply for the $n = 1$ island and thus we cannot use it to remove the peak at $v \approx 3.5$ while keeping the one at $v \approx 1.8$. However, we can exploit that for a large amplitude the $n = 1$ island tends to cover a larger range of phases in the PSS. Hence, a small phase shift in the driving law removes relatively fewer particles in the $n = 1$ island compared to the ones with higher n. Following this idea, we choose $d_B(t) = A_{101}[\cos(2.2t + \varphi_B) + \sin(4.4t + 2.2\varphi_B)]$ for $101 < B < 501$ with $\varphi_B = 0.02\pi(B - 100)$ and the resulting velocity distribution at $x = 500NL$ is shown in the inset of Fig. 9(b). Again, we obtain the desired distribution of a monoenergetic particle beam.

VII. CONCLUSION

We have explored the classical nonequilibrium dynamics of particles in a one-dimensional driven superlattice which consists of blocks, each containing many individual barriers. While similar systems that are usually studied in this context consist of lattices where all barriers are governed by the same time-dependent force, that is, driving law, we allowed for a different driving in each block. In doing so we show that the thus obtained variability leads to remarkable new dynamical phenomena. To this end we analyzed in detail how the blockwise variation of the driving law gives rise to conversion processes from diffusive to ballistic motion and vice versa at the interfaces, that is, the positions in the superlattice where the driving law changes. The combination of directed transport and these conversion processes enabled us to obtain peaked velocity distributions in a simple system containing only two blocks with different driving laws providing oppositely directed currents. Additionally, we observed strong correlations between the phases and velocities for the escaping particles, even though the initial particle ensemble is of exclusively diffusive character. Even more, we found that the velocity distributions as well as the correlations can be modified in a controlled manner by adjusting parameters such as frequency or amplitude in the driving. Finally, we present a scheme for superlattices containing a few hundred blocks by which a diffusive particle ensemble can be converted into a pulsed particle beam, whose mean energy and width in momentum space can be adjusted. Since this scheme mostly depends on simple symmetry arguments it is viable over a wide range of parameters. Thus, it should be applicable to experimental setups, such as layered semiconductor heterostructures with different ac drivings or even to cold atom experiments in which counterpropagating laser beams can create a one-dimensional lattice potential. By passing the laser beams through two acousto-optical modulators the desired ac drivings can be obtained.

As a future perspective it would be intriguing to explore—both theoretically as well as experimentally—the analogs of the presented effects in the quantum regime.

ACKNOWLEDGMENTS

C.P. and B.L. thank the Excellence Cluster Frontiers in Quantum Photon science, which is supported by the Joachim Herz Stiftung, for financial funding. We thank F. K. Diakonos for helpful discussions.

[1] S. Wiggins, *Chaotic Transport in Dynamical Systems* (Springer, Berlin, 1992).

[2] J. Maddox, Nature (London) **365**, 203 (1993).

[3] R. Bartussek, P. Hänggi, and J. G. Kissner, Europhys. Lett. **28**, 459 (1994).

[4] M. I. Dykman, H. Rabitz, V. N. Smelyanskiy, and B. E. Vugmeister, Phys. Rev. Lett. **79**, 1178 (1997).

[5] M. O. Magnasco, Phys. Rev. Lett. **71**, 1477 (1993).

[6] F. Jülicher, A. Ajdari, and J. Prost, Rev. Mod. Phys. **69**, 1269 (1997).

[7] A. V. Ponomarev, S. Denisov, and P. Hänggi, Phys. Rev. Lett. **102**, 230601 (2009).

[8] S. Flach, O. Yevtushenko, and Y. Zolotaryuk, Phys. Rev. Lett. **84**, 2358 (2000).

[9] T. Dittrich, R. Ketzmerick, M.-F. Otto, and H. Schanz, Ann. Phys. **9**, 755 (2000).

[10] S. Denisov and S. Flach, Phys. Rev. E **64**, 056236 (2001).

[11] O. Yevtushenko, S. Flach, Y. Zolotaryuk, and A. A. Ovchinnikow, Europhys. Lett. **54**, 141 (2001).

[12] S. Denisov, S. Flach, A. A. Ovchinnikov, O. Yevtushenko, and Y. Zolotaryuk, Phys. Rev. E **66**, 041104 (2002).

[13] S. Denisov, S. Flach, and P. Hänggi, Europhys. Lett. **74**, 588 (2006).

[14] J. Gong and P. Brumer, Phys. Rev. Lett. **97**, 240602 (2006).

[15] L. Wang, G. Benenti, G. Casati, and B. Li, Phys. Rev. Lett. **99**, 244101 (2007).

[16] Special issue on Ratchets and Brownian Motors: Basics, Experiments and Applications, edited by H. Linke, Appl. Phys. A **75**, 167 (2002).

[17] H. Linke, T. E. Humphrey, A. Löfgren, A. O. Sushkov, R. Newbury, R. P. Taylor, and P. Omling, Science **286**, 2314 (1999).

[18] K. N. Alekseev, M. V. Erementchouk, and F. V. Kusmartsev, Europhys. Lett. **47**, 595 (1999).

[19] R. Gommers, S. Bergamini, and F. Renzoni, Phys. Rev. Lett. **95**, 073003 (2005).

[20] R. Gommers, S. Denisov, and F. Renzoni, Phys. Rev. Lett. **96**, 240604 (2006).

[21] T. Salger, S. Kling, T. Hecking, C. Geckeler, L. Morales-Molina, and M. Weitz, Science **326**, 1241 (2009).

[22] A. Wickenbrock, P. C. Holz, N. A. Abdul Wahab, P. Phoonthong, D. Cubero, and F. Renzoni, Phys. Rev. Lett. **108**, 020603 (2012).

[23] C. Petri, F. Lenz, F. K. Diakonos, and P. Schmelcher, Phys. Rev. E **81**, 046219 (2010).

[24] B. Liebchen, C. Petri, F. Lenz, and P. Schmelcher, Europhys. Lett. **94**, 40001 (2011).

[25] C. Petri, F. Lenz, B. Liebchen, F. K. Diakonos, and P. Schmelcher, Europhys. Lett. **95**, 30005 (2011).

[26] P. Olbrich, J. Karch, E. L. Ivchenko, J. Kamann, B. März, M. Fehrenbacher, D. Weiss, and S. D. Ganichev, Phys. Rev. B **83**, 165320 (2011).

[27] E. L. Ivchenkoa and S. D. Ganichev, JETP Lett. **93**, 673 (2011).

[28] A. J. Lichtenberg and M. A. Lieberman, *Regular and Chaotic Dynamics*, 2nd ed. (Springer-Verlag, Heidelberg, 1992).

[29] N. R. Quintero, José A. Cuesta, and Renato Alvarez-Nodarse, Phys. Rev. E **81**, 030102 (2010).